Application of a new model for bubble-induced turbulence to bubbly flows in containers and vertical pipes

Liao, Y.; Ma, T.; Krepper, E.; Lucas, D.; Fröhlich, J.;

Originally published:

March 2019

Chemical Engineering Science 202(2019), 55-69

DOI: https://doi.org/10.1016/j.ces.2019.03.007

Perma-Link to Publication Repository of HZDR:

https://www.hzdr.de/publications/Publ-28589

Application of a new model for bubble-induced turbulence to bubbly flows in containers and vertical pipes

Yixiang Liao[*a], Tian Ma [a], Eckhard Krepper [a], Dirk Lucas [a], Jochen Fröhlich [b]

[a] Helmholtz-Zentrum Dresden - Rossendorf, Institute of Fluid Dynamics, Dresden, Germany

[b] Technische Universität Dresden, Institute of Fluid Mechanics, Dresden, Germany

Abstract

The present paper extends the baseline model for the CFD-simulation of turbulent poly-disperse bubbly flows in the Euler-Euler framework by improving the modelling of bubble-induced turbulence. The closure terms in the transport equations of the k-ω SST model are revisited and replaced with a new model recently proposed by Ma et al. (Ma et al., Physical Review Fluids 2, 034301, 2017) which is based on an analysis of the turbulent kinetic energy budget obtained from direct numerical simulation data. Detailed validation results for various flow configurations with a wide range of gas and liquid volumetric fluxes are presented. In case of vertical pipe flow significant improvements in the predicted gas volume fraction and velocity profiles are obtained, especially in high gas volume fraction cases where bubble-induced turbulence is dominant. Simulations of other configurations, such as uniform and non-uniform bubble columns, show that the new model results in an also for these cases overall improvement. Therefore, the baseline model is now updated to include the new model for bubble-induced turbulence.

Keywords
Bubbly flow; Bubble-induced turbulence; Euler-Euler modelling; Baseline model

1. Introduction

Turbulent bubbly flows occur in a variety of chemical, biochemical, electrochemical and energy converting industrial processes. It is known from experiments and simulations that the spatial distribution of phases in such configurations not only depends on the liquid flow fields, but also on bubble sizes. Bubbles usually exhibit a size distribution which generally changes in space and time. For example, in case of an upward co-current pipe or channel flow, small bubbles migrate to the wall while large bubbles move to the center due to the effect of lateral lift force acting differently on different size classes, thus introducing a de-mixing effect (Tomiyama, 2002; Lucas and Tomiyama, 2011, Santarelli and Fröhlich, 2016). Additional changes occur due to bubble coalescence and breakup (Liao et al., 2015) as well as phase change (Liao and Lucas, 2016). For all these processes, the level of fluid turbulence is decisive since it influences interfacial momentum transfer and bubble dynamics. In particular, the mechanism of turbulence production and dissipation becomes much more complex than in single-phase flow. According to Hosokawa and Tomiyama (2010), liquid turbulence in bubbly flows may be affected by bubbles in the

[*] Corresponding author, Dr. Yixiang Liao (Tel. +49 351 2602389, Email: y.liao@hzdr.de)

following ways: a) production due to the work of interfacial forces; b) dissipation due to the breakup of turbulence eddies by bubbles; c) change of the mean velocity profile due to interphase momentum transfer resulting in an alteration of the single-phase mechanisms of shear-induced turbulence (SIT). Kataoka et al. (1993) suggested that, additionally, small structures that may exist on the bubble surface, like wrinkles and ripples, and bubble deformation also contribute to the destruction of turbulence.

Turbulence modelling in bubbly flows remains a huge challenge mainly due to the lack of models that appropriately account for the numerous interactions between bubble motion and liquid velocity. The two- or multi-fluid model with the RANS equations for turbulence modelling is so far the most widely used approach for large scale applications due to low computational costs, but the accuracy of results depends on the closure models. Among these, the bubble-induced turbulence (BIT) appears to be the most important and is addressed in the present study. In fact, a literature survey shows that no consensus has been reached so far on how to model this effect at best. Most of the effort has focused on devising a turbulent viscosity to account for the impact of the bubbles on the Reynolds stresses (Ilić, 2006; Vaidheeswaren and Hibiki, 2017). The simplest way is to define an effective turbulence viscosity as a linear superposition of a shear-induced contribution, equivalent to the single-phase term, and a bubble-induced component in the form of an algebraic expression. The BIT viscosity model proposed by Sato and Sakoguchi (1975) employs the bubble size and the relative velocity of the bubbles with respect to the local fluid velocity as the length and velocity scale, respectively. This model has been widely adopted in a variety of scenarios by Pan et al. (1999), Deen et al. (2001), Bove and Solberg (2004), Lucas et al. (2007), Krepper et al. (2009), Rabha et al. (2013) and Scott et al. (2014), for example. Further applications are listed in Vaidheeswaren and Hibiki (2017). These authors, however, point out that the linear-superposition approach fails in representing the non-linear interactions between the shear-induced vortices and the bubbles or the wakes behind them. Furthermore, Liao and Lucas (2012) reported that in addition to providing a turbulent viscosity for the momentum equation it is necessary to predict the turbulent kinetic energy and the dissipation rate accurately since these are important input parameters for other closure models, e.g. bubble coalescence and breakup. This motivates to take the next level of complexity and determine the turbulent kinetic energy from a transport equation. The eddy viscosity is then obtained with a two-equation RANS model. Both transport equations, however, require additional source terms which are part of the model. In this way, the effect of bubbles on momentum transfer as well as the transfer of turbulent kinetic energy between the phases is accounted for, which is consistent with the views of Hosokawa and Tomiyama (2010) and Kataoka et al. (1993) mentioned above. This type of approach was first proposed by Kataoka and Serizawa (1989) and has received significant attention from many researchers. Developments were proposed by Yao and Morel (2004), Pfleger and Becker (2001), Troshko and Hassan (2001), Rzehak and Krepper (2013), among others. The present work focuses on the application of the recently developed model of Ma et al. (2017) which is based on a consistent analysis of DNS data for vertical channel flows (Santarelli and Fröhlich, 2016, Santarelli et al., 2016).

2. The k-ω-SST with BIT source terms

The transport equations for the liquid turbulent kinetic energy k and the eddy frequency ω are expressed as (Menter, 1994; Liao et al., 2011)

$$\frac{\partial}{\partial t}\left(\alpha_l \rho_l k\right) + \nabla \cdot \left(\alpha_l \rho_l \mathbf{u}_l k\right) = \nabla \cdot \left[\alpha_l \left(\mu_l + \frac{\mu_{t,l}}{\sigma_{k3}} \right) \nabla k \right] + \alpha_l P_k - \beta' \alpha_l \rho_l k \omega + S_k \ , \tag{1}$$

$$\frac{\partial}{\partial t}\left(\alpha_l \rho_l \omega\right) + \nabla \cdot \left(\alpha_l \rho_l \mathbf{u}_l \omega\right) =$$
$$\nabla \cdot \left[\alpha_l \left(\mu_l + \frac{\mu_{t,l}}{\sigma_{\omega 3}} \right) \nabla \omega \right] + \left(1 - F_1\right) 2 \alpha_l \rho_l \frac{\nabla k \nabla \omega}{\sigma_{\omega 2} \omega} + a_3 \alpha_l \frac{\omega}{k} P_k - \beta_3 \alpha_l \rho_l \omega^2 + S_\omega \ . \tag{2}$$

Here, ρ_l is the liquid density and α_l the liquid volume fraction. The term P_k designates the SIT production, while S_k and S_ω are BIT sources terms, for which a number of models are available in the literature.

To maintain the coherence of the text some of them will be discussed here in more detail. Most of the models assume the energy input by the interphase drag force as the major source of BIT, while the contributions of other forces are neglected. The following expression is based on Kataoka and Serizawa (1993)

$$S_k = C_k \left|\mathbf{F}_D\right| \left|\mathbf{u}_{rel}\right| = C_k \frac{3}{4} \rho_l \frac{C_D}{d} \left|\mathbf{u}_{rel}\right|^3 , \tag{3}$$

where C_D, $\mathbf{F}_D$, d, $\mathbf{u}_{rel}$ are the drag coefficient, the interphase drag force, the bubble diameter and the relative velocity vector, respectively, while C_k is a model constant.

To model the BIT source term S_ω, a link is established to the source term in the dissipation rate equation, S_ε. The latter is obtained in the same way as for single-phase flow, with the BIT-source term for the turbulence dissipation assumed to be proportional to the source of turbulent kinetic energy divided by a characteristic time scale, τ, i.e. (Morel, 1997; Politano et al, 2003)

$$S_\varepsilon = C_\varepsilon \frac{S_k}{\tau} . \tag{4}$$

The source term for the ω-equation is then obtained from S_k and S_ε according to the relation between k, ω and ε (Rzehak and Krepper, 2013; Liao and Lucas, 2015)

$$S_\omega = \frac{1}{\beta' k} S_\varepsilon - \frac{\omega}{k} S_k . \tag{5}$$

For the model constants σ_{k3}, $\sigma_{\omega 2}$, $\sigma_{\omega 3}$, β', α_3, β_3 the standard values for single phase flow are used.

The main difference between the BIT source term models lies in the expressions for the time scale τ in Eq. (4). The time scale for BIT dissipation is usually different from the one characterizing single-phase turbulence, which implies that the process of turbulence generation and disappearance in two-phase flows is a problem with two time scales. Rzehak and Krepper (2013) suggested that two characteristic length and velocity scales are present in a two-phase flow, one related to the bubbles, the other related to energy-containing turbulence eddies.

Consequently, on the basis of dimensional analysis four time scales τ_1 to τ_4 may be formed, as defined in Table 1. A fifth time scale is added, based on the assumption that the bubble-induced eddies have a size λ proportional to the bubble diameter d and they are in the inertial subrange of turbulence having a velocity $(\varepsilon\lambda)^{1/3}$, as detailed below.

Table 1 Characteristic scales in two-phase flows

Length scale l	Velocity scale u	Time scale τ
$k^{3/2}/\varepsilon$	$\sqrt{k}$	$\tau_1 = \frac{k}{\varepsilon}$
		$\tau_2 = \frac{k^{3/2}}{\varepsilon \lvert \mathbf{u}_{rel} \rvert}$
d	$\lvert \mathbf{u}_{rel} \rvert$	$\tau_3 = \frac{d}{\sqrt{k}}$
		$\tau_4 = \frac{d}{\lvert \mathbf{u}_{rel} \rvert}$
$\lambda \sim d$	$(\varepsilon\lambda)^{1/3}$	$\tau_5 = \frac{d^{2/3}}{\varepsilon^{1/3}}$

The time scale τ_1 is identical with the one for single phase flow and does not contain any bubble information. It is used in the BIT models of Pfleger and Becker (2001) and Politano et al. (2003). The mixed time scale τ_2 can be decomposed into the single phase time scale multiplied by the ratio of the turbulent velocity to the bubble relative velocity. It turned out to cause convergence difficulties of the numerical solution and was dropped from further consideration by Rzehak and Krepper (2013). The time scale τ_3 combines the bubble size with the turbulent kinetic energy and is the one retained by Rzehak and Krepper (2013). A similar one was proposed by Yao and Morel (2004), who argued that the bubble size is more suitable than the eddy size for the characterization of BIT in the wake behind a bubble. In addition, eddies induced by bubbles should have a size equivalent to the bubble size and are in the inertial subrange instead of the energy-containing one. Thus, the time scale in the model of Yao and Morel (2004) has the form of τ_5 in Table 1 and depends on the dissipation rate of turbulent kinetic energy. Time scale τ_4 is free of turbulence parameters, which is consistent with the view of Lopez de Bertodano (1992), who considered the dependence of BIT dissipation on turbulence parameters in τ_1, τ_2, τ_3 and τ_5 as unreasonable due to an unexpected dependence on the initial conditions. The time scale τ_4 was used by Troshko and Hassan (2001) and Ma et al. (2017) for the establishment of their models. Furthermore, by analyzing the energy spectra of DNS and experimental data Ma et al. (2017) concluded that this time scale might be better suited for characterizing the BIT than the other alternatives listed in Table 1, since they are in the typical −3 range of the energy spectra in the presence of BIT.

Besides the time scale also the choice of the two pre-factors in Eq. (3) and Eq. (4), C_k and C_ε, is an open issue in the literature. According to Rzehak and Krepper (2013) these coefficients are not necessarily constants. They may be related to some dimensionless variables or numbers, but

knowledge on the functional dependencies is still insufficient. As a result, they are often taken as constants, and different values have been used, some of which are listed in Table 2.

Table 2 Pre-factors C_k and C_ε in different BIT models

	Troshko & Hassen (2001)	Politano et al. (2003)	Yao & Morel (2004)	Rzehak & Krepper (2013)
C_k	1.0	1.0	1.0	1.0
C_ε	0.45	1.92	0.6	1.0

The factor C_k should be smaller than or equal to 1.0, since in case C_k=1.0 all the available energy transferred by the drag force that does not drive the mean liquid flow would be transformed into turbulent kinetic energy (Ma et al., 2017). Concerning C_ε, it is observed that Končar et al. (2005) adopted the model of Yao and Morel (2004) in simulations of subcooled flow boiling and varied the value of C_ε. They found a clear effect on void fraction and velocity profiles. Similar results were obtained by Rzehak and Krepper (2013) who has to use different values of C_ε for air-water bubbly flow through vertical pipes of different sizes. For example, a value of 2 gave better agreement with the data of Liu (1998) while for the Shawkat et al. (2008) experiments the reduction of C_ε to 0.5 was necessary. However, for the tests of Hosokawa et al. (2007) it was impossible to get an overall improvement with a single C_ε. Therefore, they recommended a value of 1.0 for general purpose. The need of tuning is predominantly due to the fact that not all relevant physical effects are represented in these models. This issue restricts the reliability and accuracy of the simulation results.

On this background, Ma et al. (2017) used the DNS database on bubbly channel flow by Santarelli and Fröhlich (2016), Santarelli et al. (2016), mentioned above, to determine these pre-factors in a more consistent way. Ma et al. (2017) developed a functional dependency of C_k and C_ε on the particle Reynolds number Re_p and the drag coefficient C_D of the form

$$C_k = \min\left(0.18\,\mathrm{Re}_p^{\,0.23},\ 1\right), \tag{5}$$

$$C_\varepsilon = 0.3 C_D . \tag{6}$$

The present work is devoted to applying this BIT modeling within the baseline model to a wider class of flows and to assess whether and by how much this improves the results.

3. The baseline model for poly-disperse bubbly flows

To close the two- or multi-fluid conservation equations, closures are required that reflect the unresolved local phenomena like interphase mass, momentum and energy transfer, turbulence, as well as bubble coalescence and breakup. For the various specific phenomena to be tackled a large number of different model expressions can be found in the literature. Papers on corresponding CFD simulations often present simulations of a single or few experiments only with particular combinations of sub-models, so that the results are hardly comparable across

articles and the acquired knowledge and experience is not transferable to other cases, even if these are similar.

To improve the situation, a baseline model was proposed by Lucas et al. (2016). With this approach, a fixed set of closure models was defined for two- or multi-fluid modelling of bubbly flows with bubbles in the range from 1 mm to about 15 mm size, in terms of the volume-equivalent diameter, and applied to a large number of cases without any modification. In this way the interference of model-related uncertainties and user-dependent tuning can be minimized. The aim of the baseline model is to establish an interactive procedure for model development, and a common basis for researchers sharing their experience. The long-term goal is to extend the generality of the models by exploring the physics and nature of local phenomena. The basic scheme of the baseline model concept is sketched in Fig. 1.

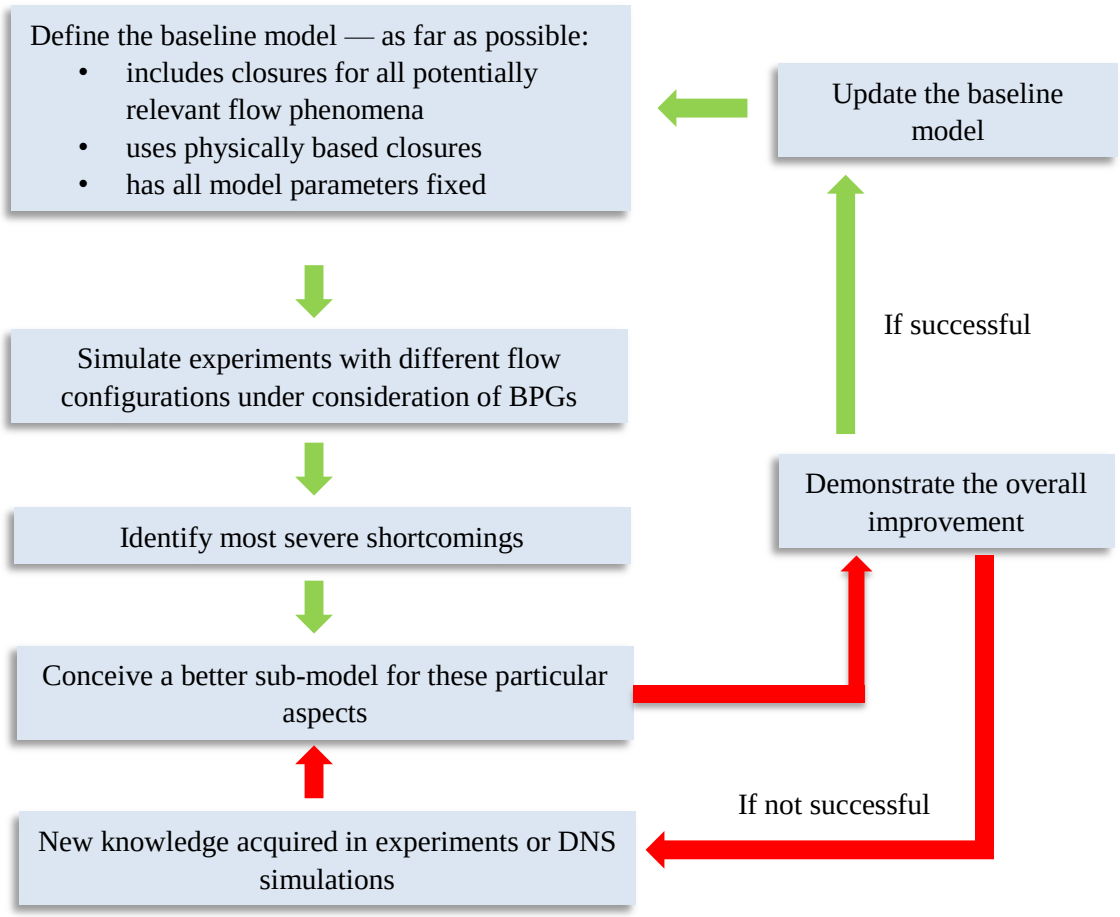

Fig. 1 HZDR baseline closure concept for model development (Liao et al., 2018a).

The baseline model is defined guided by three main principles: a) taking into account all physical phenomena relevant to bubbly flows, e.g. interphase momentum transfer, two-phase turbulence and bubble dynamics; b) using the most physically based models that are available; c) fixing all models and constants. For the purpose of validation, a database with around 150 test cases is used routinely which consists of a variety of bubbly flow systems with different configurations

and combinations of media. After a systematic analysis and evaluation of the comprehensive simulation results, the most severe shortcomings of the model are identified and reasonable hypotheses are generated for further development. On the basis of this expertise suitable laboratory experiments or DNS are designed to provide more insight and understanding of the respective phenomenon. In this way, a better sub-model with more physical knowledge for the particular aspect is developed. It is then incorporated into the baseline model and the simulation of all cases in the database is repeated. If an overall improvement is demonstrated, the new sub-model is included and the baseline model is ready to be updated. The focus of the present work is an update of the BIT sub-model.

The first version of the baseline model (hereinafter referred to as BSL-1.0) for isothermal bubbly flow takes into account interphase momentum transfer due to drag, shear lift, turbulence dispersion, virtual mass, wall force, BIT, as well as bubble coalescence and breakup. The sub-models for the description of these local phenomena are summarized in Table 3. For more details about each model the reader is referred to the original references listed in the right column.

Table 3. Sub-models contained in the first version of the baseline model (BSL-1.0)

	Term	**Model**	**Reference**
Interfacial force	drag	$\boldsymbol{F}_D = -\frac{3}{4d} C_D \rho_l \alpha_g \lvert \boldsymbol{u}_g - \boldsymbol{u}_l \rvert (\boldsymbol{u}_g - \boldsymbol{u}_l)$ $C_D = \max\left(C_{D,Sphere}, min\left(C_{D,ellipse}, C_{D,cap}\right)\right)$ $C_{D,Sphere} = \frac{24}{Re_p}\left(1 + 0.1 {Re_p}^{0.75}\right)$ $C_{D,ellipse} = \frac{2}{3} Eo^{0.5},\ C_{D,cap} = \frac{8}{3}$	Ishii and Zuber (1979)
	shear lift	$\boldsymbol{F}_L = -C_L \rho_l \alpha_g \left(\boldsymbol{u}_g - \boldsymbol{u}_l\right) \times rot(\boldsymbol{u}_l)$ $C_L = \begin{cases} \min\left[0.288 \tanh(0.121 Re_p, f(Eo_\perp)\right] & Eo_\perp < 4 \\ f(Eo_\perp) & 4 \le Eo_\perp < 10 \\ -0.27 & Eo_\perp \ge 10 \end{cases}$ $f(Eo_\perp) = 0.00105 Eo_\perp^3 - 0.0159 Eo_\perp^2 - 0.0204 Eo_\perp + 0.474$ $Eo_\perp = \frac{g(\rho_L - \rho_G) d_\perp^2}{\sigma},\ d_\perp = d\sqrt[3]{1 + 0.163 Eo^{0.757}}$	Tomiyama et al. (2002)
	turbulent dispersion	$\boldsymbol{F}_{TD} = -\frac{3}{4} C_D \frac{\alpha_g}{d} \lvert \boldsymbol{u}_g - \boldsymbol{u}_l \rvert \frac{\mu_{t,l}}{Pr_t}\left(\frac{1}{\alpha_l} + \frac{1}{\alpha_g}\right) \nabla \alpha_g$	Burns et al. (2004)
	virtual mass	$\boldsymbol{F}_{VM} = -C_{VM} \alpha_g \rho_l \left(\frac{D_g \boldsymbol{u}_g}{Dt} - \frac{D_l \boldsymbol{u}_l}{Dt}\right),\quad C_{VM} = 0.5$	Crowe et al. (2012)
	wall force	$\boldsymbol{F}_W = \frac{2}{d} C_W \rho_l \lvert \boldsymbol{u}_g - \boldsymbol{u}_l \rvert^2 \boldsymbol{n}_w$ $C_W = f(Eo)\left(\frac{d}{2y}\right)^2,\quad f(Eo) = 0.0217 Eo$	Hosokawa et al. (2002)
Turbulence	liquid	$\frac{\partial}{\partial t}(\alpha_l \rho_l k) + \nabla \cdot (\alpha_l \rho_l \boldsymbol{u}_l k) = \nabla \cdot \left[\alpha_l \left(\mu_l + \frac{\mu_{t,l}}{\sigma_{k3}}\right) \nabla k\right] + \alpha_l P_k - \beta' \alpha_l \rho_l k \omega + S_k$	Menter (1994) ANSYS (2012)

		$\frac{\partial}{\partial t}(\alpha_l\rho_l\omega) + \nabla\cdot(\alpha_l\rho_l\boldsymbol{u}_l\omega)$ $= \nabla\cdot\left[\alpha_l\left(\mu_l + \frac{\mu_{t,l}}{\sigma_{\omega 3}}\right)\nabla\omega\right]$ $+ (1-F_1)2\alpha_l\rho_l\frac{\nabla k\nabla\omega}{\sigma_{\omega 2}\omega} + a_3\frac{\omega}{k}\alpha_l P_k - \beta_3\alpha_l\rho_l\omega^2$ $+ S_\omega$ $\nu_{t,l} = \frac{a_1 k}{max(a_1\omega,\ SF_2)}$	
	BIT	$S_k = C_k\frac{3}{4}\rho_l\frac{C_D}{d}\lvert\boldsymbol{u}_{rel}\rvert^3,\quad S_\varepsilon = C_\epsilon\frac{S_k}{\tau},$ $S_\omega = \frac{1}{C_\mu k}S_k - \frac{\omega}{k}\varphi_\varepsilon,\quad \tau = \frac{\mathrm{d}}{\sqrt{k}}$	Rzehak and Krepper (2013)
	gas	$\nu_{t,g} = \nu_{t,l}$	
Poly-dispersity	population balance model	MUSIG model: $\frac{\partial}{\partial t}(\alpha_g\rho_g f_i) + \nabla\cdot(\alpha_g\rho_g u_g f_i) = B_{Bi} - D_{Bi} + B_{Ci} - D_{Ci}$ $B_{Bi} = \alpha_g\rho_g\left[\sum_{j\geq i}\frac{m_i}{m_j^2}\left(\Omega(m_j,m_i)f_i\Delta m_{ij} + \sum_{k=1}^{M}\Omega(m_j,m_k)f_j\Delta m_{kj}Y_{jki}\right)\right]$ $D_{Bi} = \alpha_g\rho_g\frac{1}{m_i}\sum_{j=1}^{i}\Omega(m_i,m_j)f_i\Delta m_{ji}$ $B_{Ci} = \frac{1}{2}(\alpha_g\rho_g)^2\sum_{j\leq i}\sum_{k\leq i}\Gamma(m_j,m_k)X_{jki}f_i f_k\frac{m_i}{m_j m_k}$ $D_{Ci} = (\alpha_g\rho_g)^2 f_i\sum_j\Gamma(m_i,m_j)f_j\frac{1}{m_j}$	Krepper et al. (2008) Liao et al. (2018b)
	coalescence and breakup	$\Gamma(m_i,m_j)$ $= \frac{\alpha_{g,max}}{\alpha_{g,max}-\alpha_g}\begin{cases}\frac{\pi}{4}(d_i+d_j)^2\lvert\boldsymbol{u}_{rel,turb}\rvert\lambda_{inertial} & (d_i+d_j>\eta)\\ \frac{\pi}{8}(d_i+d_j)^2\lvert\boldsymbol{u}_{rel,eddy}\rvert\lambda_{viscous} & (d_i+d_j>\eta)\\ \frac{\pi}{8}(d_i+d_j)^2\lvert\boldsymbol{u}_{rel,shear}\rvert\lambda_{eff}\\ \frac{\pi}{8}(d_i+d_j)^2\lvert\boldsymbol{u}_{rel,buoy}\rvert\lambda_{eff}\\ \frac{\pi}{8}(\lvert\boldsymbol{u}_{rel,wake,i}\rvert\Theta_i + \lvert\boldsymbol{u}_{rel,wake,j}\rvert\Theta_j)\end{cases}$ where $\boldsymbol{u}_{rel,turb}$, $\boldsymbol{u}_{rel,eddy}$, $\boldsymbol{u}_{rel,shear}$, $\boldsymbol{u}_{rel,buoy}$, $\boldsymbol{u}_{rel,wake,i}$ are relative velocity between bubbles caused by turbulence fluctuation, shear, buoyancy and wake. $\Omega(m_i,m_j) = \frac{1}{d_i\sqrt{\rho_l}}(\sqrt{\tau_{turb}-\tau_{crit}} + \sqrt{\tau_{shear}-\tau_{crit}} + \sqrt{\tau_{eddy}-\tau_{crit}} + \sqrt{\tau_{fric}-\tau_{crit}})$	Liao et al. (2015)

		$\tau_{crit} = max\left(\frac{6\sigma}{d_i}\left(\left(\frac{d_j}{d_i}\right)^2 + \left(\frac{\left({d_i}^3 - {d_j}^3\right)^{1/3}}{d_i}\right)^2 - 1\right), \frac{\sigma}{min\left(d_j,\ \left({d_i}^3 - {d_j}^3\right)^{1/3}\right)}\right)$ where τ_{turb}, τ_{shear}, τ_{eddy}, τ_{fric} are destroying stresses acting on a bubble caused by turbulence, shear and buoyancy.	

The BSL-1.0 model was tested for a large number of bubbly flow configurations, ranging from pipe flow, bubble column, airlift reactor to a stirred tank. Its generality for cases with relatively small bubble size and low gas volume fraction was shown by Rzehak et al. (2017) and Ziegenhein et al. (2017). However, in simulations of vertical pipe flows a severe shortcoming was identified in cases with large bubbles that migrate to the pipe center due to the effect of the lift force. An excessive accumulation of these bubbles often appears in the pipe center region (r/R≈0), and a fluctuating unstable radial profile of gas volume fraction is observed in the steady-state cases. As an example, the results of two test cases, MT094 and MT096, from the MT-Loop experiments are shown in Fig. 2a) and 2b), respectively. More details about the experiments and the test cases will be given in the next section. The simulations were performed with two dispersed phases, small bubbles (d<6 mm) and large bubbles (d>6 mm). In both cases, the fully-developed distribution of small bubbles at the top of the pipe (L = 3.03m) agrees well with the measurement, while the concentration of large bubbles in the pipe center is significantly over-predicted.

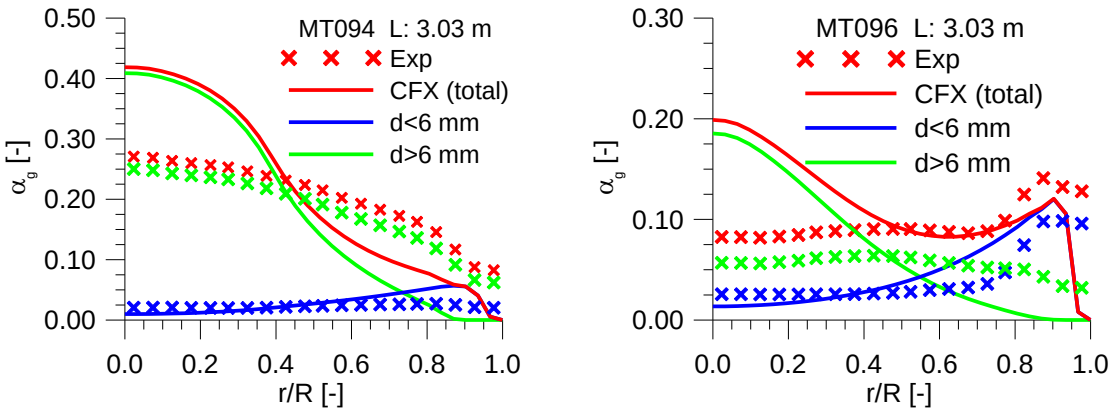

Fig. 2 Predicted and measured radial gas volume fraction profiles at the top of a vertical pipe flow. a) MT094: J_l= 0.405 m/s, J_g=0.0898 m/s, b) MT096: J_l= 1.0167 m/s, J_g=0.0898 m/s

In this work the terms “large” and “small” bubbles designate bubbles with a mean size larger or smaller, respectively, than the critical bubble size at which the lift force changes its sign. This critical size is about 6 mm for air-water systems under normal conditions according to the correlation of Tomiyama et al. (2002) reproduced in Fig. 3.

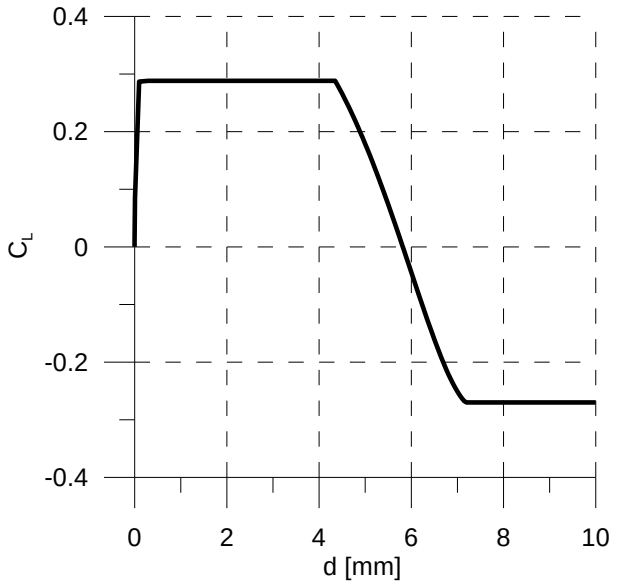

Fig. 3 Dependency of lift force coefficient on volume-equivalent bubble diameter according to Tomiyama et al. (2002).

In fully developed bubbly flows the lateral gas volume fraction profile is mainly determined by the equilibrium of non-drag forces in the lateral direction. Thereof, turbulence dispersion and lift force are the major contributions acting on the bubbles in the pipe center region. The pronounced core peak appearing in the profile of large bubbles (d>6 mm) and the total gas phase shown in Fig. 2 is supposed to be caused by a too small turbulent dispersion force in comparison with the lateral lift force. Although the bubble size has proven to affect the force balance and the radial void fraction profiles significantly (Liao et al., 2015), such an insufficient turbulence dispersion force may be related to an under-prediction of turbulence viscosity. Independently from the uncertainties involved in the prediction for the lift force using the model of Tomiyama et al. (2002), application of a more physics-based BIT model is of great interest. In comparison with the one currently included in the baseline model, which is purely based on dimensional analysis, the model of Ma et al. (2017) introduced above has a sound physical basis and thus fits better into the baseline model strategy. For this reason, it was tested in the framework of the baseline model. Encouraging results were achieved for vertical and inclined pipe flows (Krepper et al., 2018), as well as uniform and non-uniform bubble columns and airlift reactors (Liao et al., 2018a). Further test cases will be presented in the present work, with a focus on the demonstration of an overall improvement through comparisons with the results obtained by the baseline model BSL-1.0. The updated version including the BIT model of Ma et al. (2017) is referred to as BSL-2.0 in the following.

4. Investigated cases and simulation setup

To assess the BIT modelling presented above, a large number of fully-developed bubbly flows in vertical pipes and bubble columns is investigated by performing monodisperse two-fluid simulations using ANSYS CFX as a platform. The 15 air-water test cases cover a relatively broad range of superficial gas and liquid velocities (J_g=0.015 to 0.14 m/s, J_l=0.0 to 1.067 m/s), a bubble size in the range 3 to 8 mm, and a volume fraction range of 1 to 22%. An overview of the experimental conditions is given in Table 4. They include databases on bubbly flows inside a

medium pipe and a large pipe, and two bubble columns, one featuring a homogeneous bubble plume, the other an oscillating bubble plume.

Table 4 Overview of the cases investigated

Configurations		**References**	**Geometry size**	**Case No.**	**J_l [m/s]**	**J_g [m/s]**	**d [mm]**	**α_g [%]**
Vertical pipe flow		MT-Loop experiments (Prasser et al., 2003; Lucas et al. 2005)	pipe diameter D=51.2mm	MT072	0.405	0.0368	5.407	6.74
				MT074	1.067	0.0368	5.645	3.90
				MT083	0.405	0.0574	6.404	13.40
				MT085	1.067	0.0574	5.550	6.59
				MT094	0.405	0.0898	7.630	17.50
				MT096	1.067	0.0898	5.832	9.90
				MT105	0.405	0.140	8.596	22.64
				MT107	1.067	0.140	6.664	13.73
		Shawkat et al. (2008)	pipe diameter D=200mm	S21	0.45	0.015	4.1	2.4
				S23	0.45	0.1	5.0	10.7
				S31	0.68	0.015	3.2	1.7
				S33	0.68	0.1	4.7	10.1
		Ohnuki and Akimoto (2000)	pipe diameter D=200mm	O1	1.06	0.11	3.6	8.0
Bubble column	uniform	Akbar et al. (2012)	rectangular cross-section 72x240mm	A1	0.0	0.003	4.37	2.0
	non-uniform	Deen et al. (2001)	rectangular W×D=150 ×150mm	D1	0.0	0.0049	4.0	1.24

For the vertical pipe flows a small cylindrical sector covering 4° of the circumference is computed instead of the whole pipe, as shown in Fig. 4, since the flow is statistically steady and axisymmetric. This small angle allows the application of a two-dimensional mesh, containing only one layer of cells in the azimuthal direction (Fig. 4c). The front and back faces of the wedge are treated as mirror-symmetric planes. Mass flow inlet conditions are used and the flow rates specified according to the experimental conditions. Pressure boundary conditions are used for the outlet, where the static pressure is atmospheric. At the wall, free-slip and no-slip velocity conditions are applied for the gas and liquid phases, respectively.

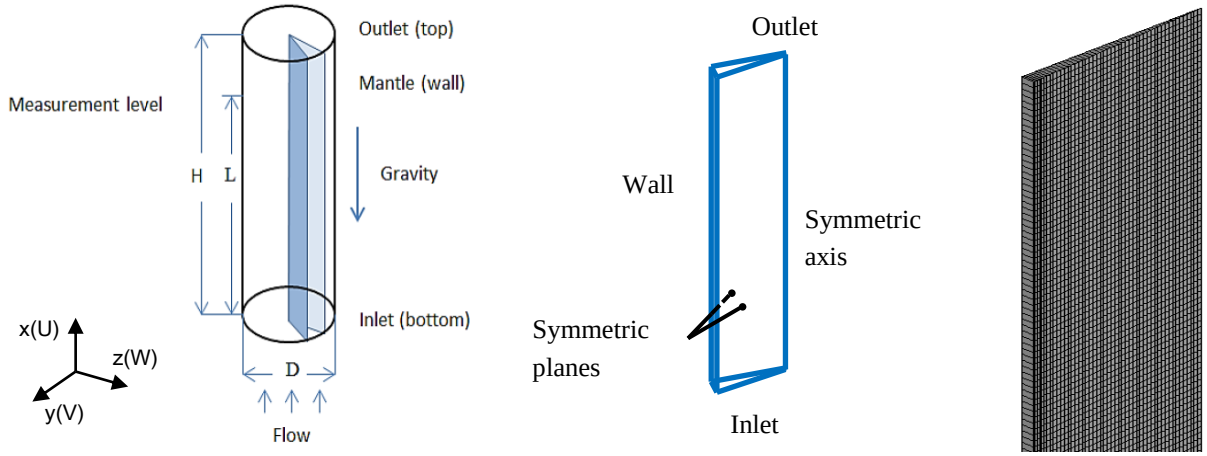

Fig. 4 Computational domain and mesh for the pipe flow cases. a) Geometry and coordinate system, b) boundary conditions, c) part of the mesh.

The geometry of the bubble column cases A1 and D1 is depicted in Fig. 5, also providing the extensions in all three directions. The inlet and wall conditions were defined in the same way as for the pipe flow cases. But, instead of a pressure outlet condition a degassing outlet condition was applied at the free surface constituting the upper boundary of the columns. This allows the gas to escape from the domain while the liquid is retained. The initial condition for the simulations was stagnant fluid without any bubbles. At t=0 air was injected through the bottom through orifices. In the case A1, the setup of Akbar et al. (2012), the injection orifices are distributed homogeneously over the whole container bottom and a uniform bubbly flow is generated (Fig. 5a). In the case D1 according to Deen et al. (2001) the gas was injected from a center area of $0.03 \times 0.03 m^2$ which leads to a bubble plume (Fig. 5b). With the parameters employed in the reference this bubble plume exhibits an oscillatory motion. To capture unsteady behavior of the bubble plumes three-dimensional transient simulations were performed for both bubble column cases. In the experiments time-averaged data were determined in the horizontal planes indicated by the red dashed line in Fig. 5. The same was done in the simulations so that comparison with the experimental data can be performed very easily.

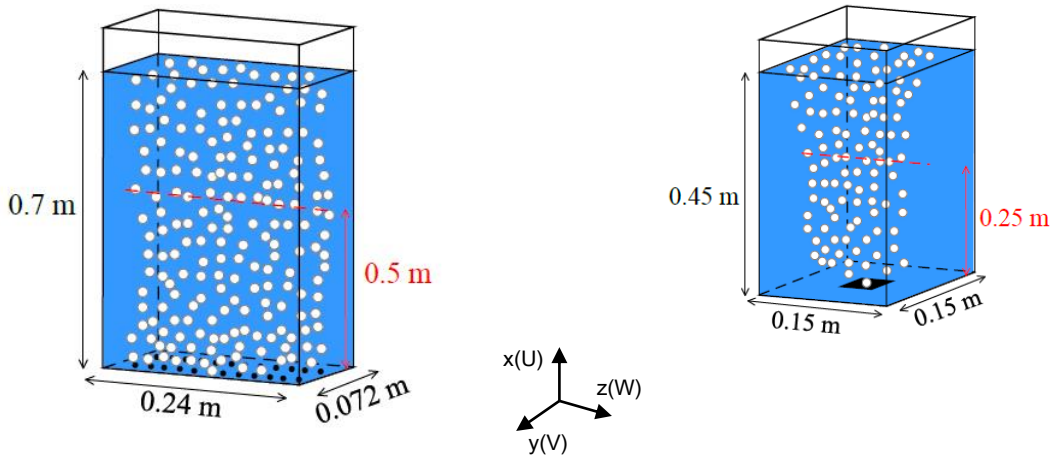

Fig. 5 Schematic description of the two bubble columns simulated. a) Case A1, homogeneous bubble column, b) Case D1, oscillating bubble plume

All simulations employed the coupled volume fraction algorithm which allows the implicit coupling of velocity, pressure and volume fraction equations with no slip imposed between gas and liquid. The high resolution scheme was selected to calculate the advection terms. Time stepping was performed with the second-order backward Euler scheme. The upwind advection and the first-order backward Euler time scheme were used for the turbulence quantities. Convergence of the simulation is identified with the maximum residual of all equations being smaller than 10^{-4}.

5. Results for vertical pipe flow

Two simulations were performed for each case in Table 4, one with the BSL-1.0 version of the baseline model, the other with the BSL-2.0. The comparison of the predictions for gas volume fraction, gas and liquid velocity as well as turbulence parameters is presented below for each of the cases.

5.1. MT-Loop cases

Radial gas volume fraction profile

In Fig. 6 the mean radial gas volume fraction profiles from the simulations are compared with the measured ones. The circles represent experimental data, while the dashed and the solid lines represent the results using the BSL-1.0 and BSL-2.0 model, respectively. The two predictions are close to each other in case of a mean bubble diameter smaller than 6 mm, e.g. in cases MT072, MT074, MT085, MT096. The ratio between gas and liquid superficial velocities is relatively small and the SIT is dominant in these cases. With the increasing superficial gas velocity or decreasing superficial liquid velocity, the proportion of BIT in the liquid turbulence increases. While the BSL-1.0 yields too large a core-peak, substantial improvement is obtained with the new BIT model, e.g. in cases MT083, MT094 and MT107, where good agreement with the

experimental data is achieved. The explanation for the improvement is that the new BIT model calculates a higher turbulent viscosity leading to a larger turbulent dispersion force so that it is sufficient to balance the accumulation effect of the lift force. In the intermediate cases, where the gas volume fraction profile changes from wall-peak to core-peak, e.g. MT085 and MT096, a slight over-prediction of the central gas volume fraction together with an under-prediction in the near-wall region is obtained with both models. This is most likely due to the prescription of a constant bubble diameter, since in these cases the bubble size stretches over the transition range (4.4 ~ 7.2 mm, see Fig. 3), where the lift force coefficient changes from positive to negative and a fine discretization of the size spectrum is necessary.

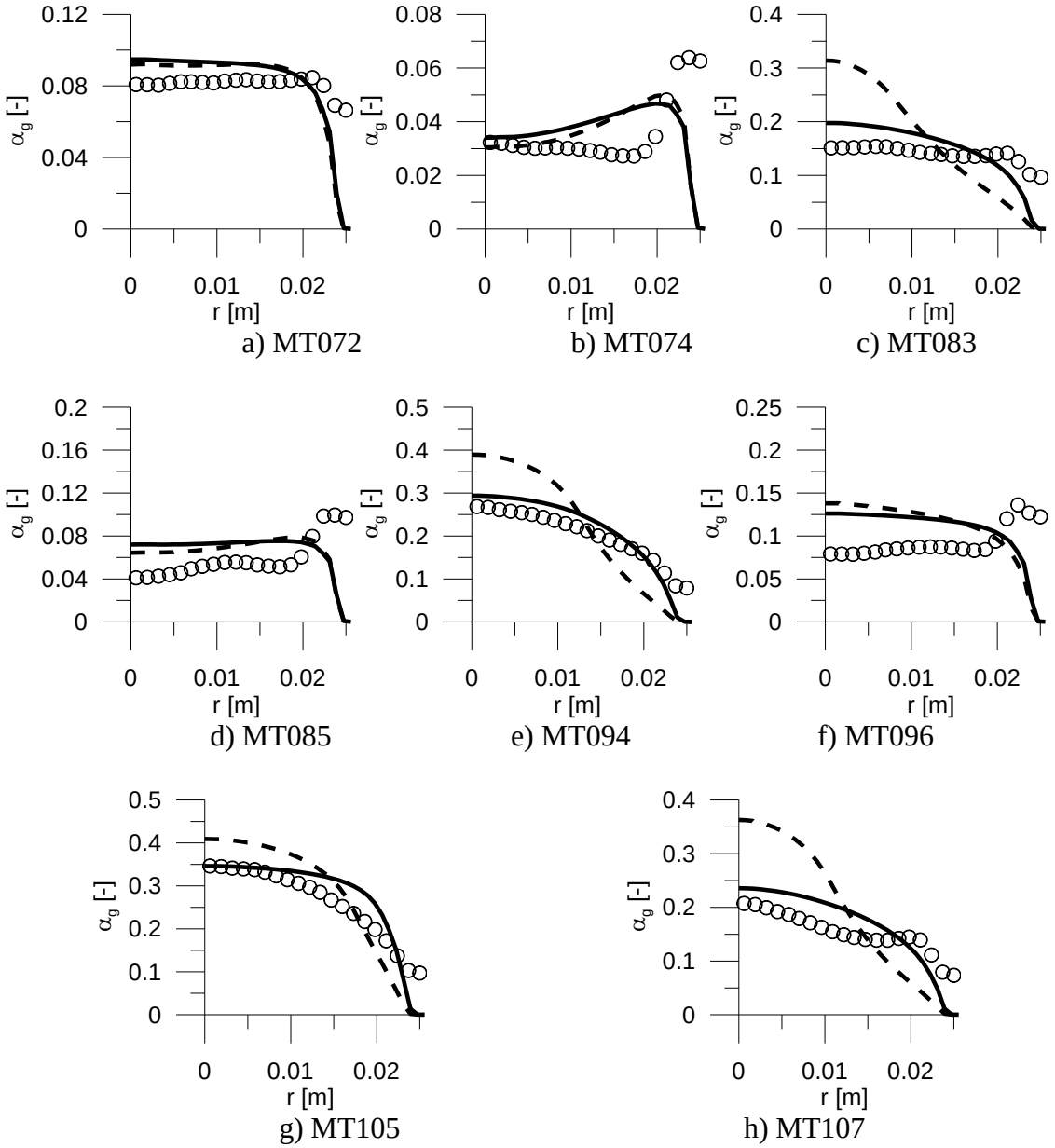

Fig. 6 Predicted and measured radial gas volume fraction profiles for MT-Loop cases (symbols: Exp., dashed line: BSL-1.0, solid line: BSL-2.0)

Gas velocity

Figure 7 shows a comparison of the radial profile of the vertical gas velocity component for the eight MT-Loop cases listed in Table 4. Both predictions are in good agreement with the experiment in case MT074, where the gas volume fraction is about 3.9% and BIT is supposed to be negligible in comparison to SIT. As the superficial liquid velocity decreases or the gas velocity increases the BSL-1.0 model (dashed line) gives a significant over-prediction of the gas volume fraction profile at the pipe center (Fig. 6). The profiles of the liquid velocity (not shown here for conciseness) have a similar shape as those of the gas velocity. The large negative gradient of the liquid velocity in radial direction increases the lift force and the accumulation of large bubbles at the center, which leads to a positive feedback between liquid velocity gradient, radial gas volume fraction profile and lift force. In contrast, the predictions of the BSL-2.0 model show a considerable improvement and coincide with the experimental data at high gas volume fraction, which demonstrates the superiority of the new BIT model for these cases.

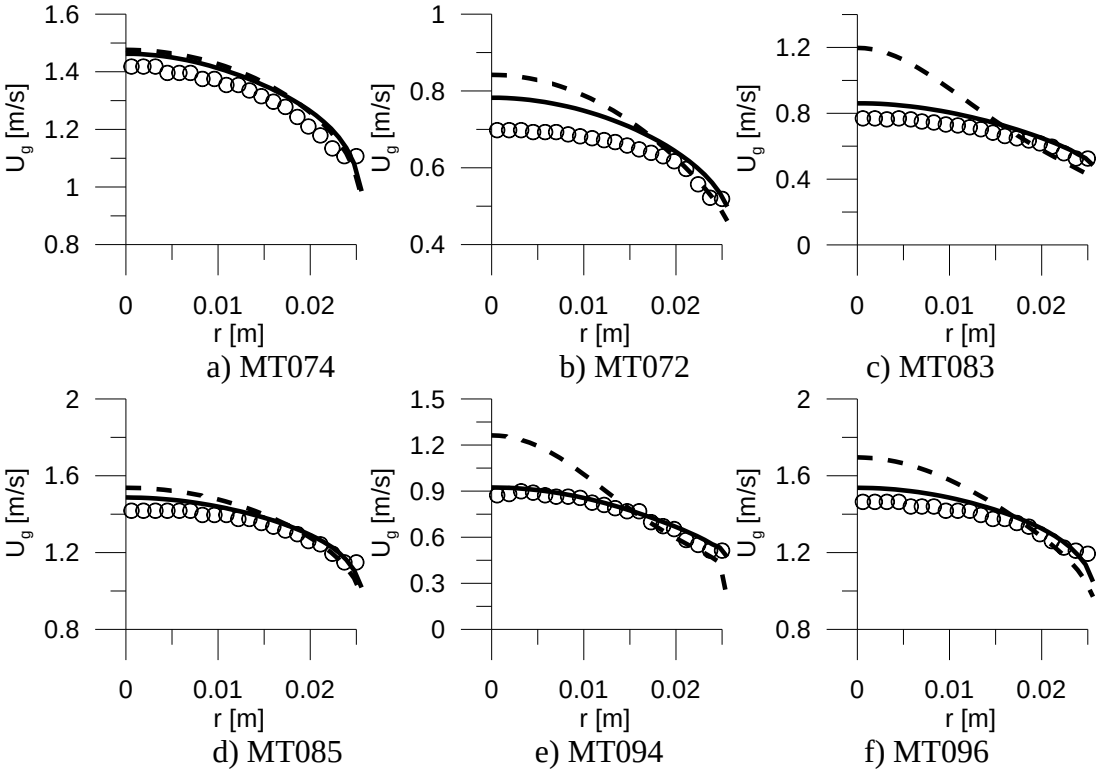

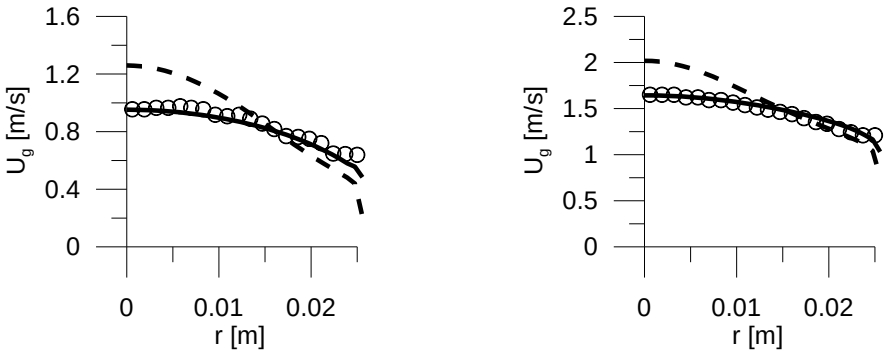

g) MT105 h) MT107

Fig. 7 Predicted and measured radial gas velocity profiles for the MT-Loop cases (symbols: Experiment, dashed line: simulation with BSL-1.0, solid line: simulation with BSL-2.0)

Unfortunately, there are no turbulence measurements available from the MT-Loop experiment which could be used for comparison. Hence, two further pipe flow experiments were simulated, for which additional information about turbulent kinetic energy and liquid velocity is available. Their setup differs from the MT-Loop experiment mainly in the diameter of the pipe.

5.2. Shawkat cases

The new model was also applied to an experiment with a pipe diameter larger by a factor of four compared to the previous subsection. Four different cases were simulated, differing by gas and liquid flow rates (Table 4). This is interesting because at the same bubble size and the same superficial gas and liquid velocities, the gas phase is distributed much more uniformly over the cross section than in cases with a small pipe diameter. This can be appreciated by comparing Fig. 6 and Fig. 8. The effect of the diameter scale on the flow pattern and the phase distribution was discussed in Oknuki and Akimoto (2000). They found that the velocity gradient in a large-scale pipe is smaller, and the smaller velocity gradient is one of the reasons for a more uniform gas volume fraction profile in the wider pipe due to a lower lift force. The cases with smaller velocity gradient and a uniform gas volume profile are preferred for validating a BIT model, since the portion of BIT is significant under these conditions.

Radial profiles of gas volume fraction

Figure 8 evidences that the flat profile prevailing in a large percentage of the pipe cross section is well reproduced by the old model, BSL-1.0. Also the wall-peak in cases S21 and S31 is captured. A peak in the near-wall region is observed in the prediction of cases S23 and S33, which is due to a positive lift force coefficient and almost not present in the experimental data. It is well established that the presence of large bubbles and the reversal in the direction of the lift force is the main reason for bubbles migrating to the pipe centerline forming a “core peak” in a large pipe. Poly-dispersity of bubbles in the experiment may be of importance here and a single mean diameter insufficient to capture the de-mixing motion of bubbles. In fact, the mean bubble size is in the range of 4 - 7 mm, where the lift coefficient changes its sign from positive to negative as shown in Fig. 3. A broad size spectrum may be present in large pipes. Unfortunately, there is no information about the bubble size distribution available from the experiment. Instead, the local

Sauter mean diameter was measured. And therefore, a simulation with a more sophisticated model to account for the lift force sign change, e.g. multi-fluid model, is difficult to conceive. In addition, Shawkat et al. (2008) and Ohnuki and Akimoto (2001) proposed that the turbulent dispersion force plays a more important role in controlling the void distribution in large diameter pipes. Further investigation on the turbulence dispersion modelling is necessary.

Now turning to the results with the new BSL-2.0 model it is obvious that the void fraction computed is fairly similar to the result with the old model. A slight improvement is seen, though, which manifests itself by a smaller overshoot in the wall peaks providing a solution somewhat closer to the experiment in all cases.

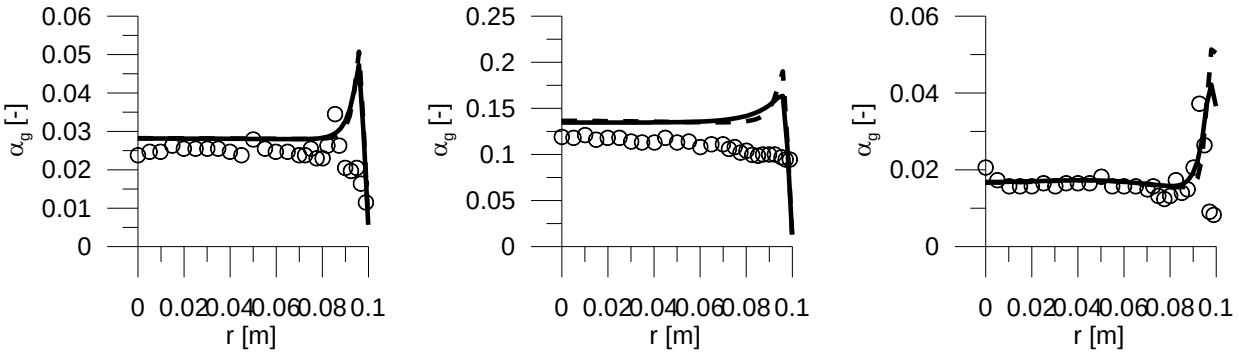

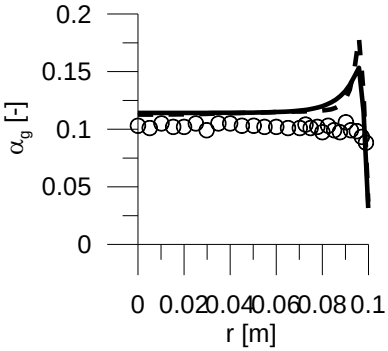

Fig. 8 Predicted and measured radial gas volume fraction profiles for the Shawkat test cases (symbol: Exp., dashed line: BSL-1.0, solid line: BSL-2.0)

Turbulent kinetic energy

Figure 9 evidences that the predictions by BSL-1.0 and BSL-2.0 coincide with each other in the cases S21 and S31. In case S21 the predicted turbulent kinetic energy agrees well with the experiment close to the pipe wall, with the sudden decrease in the measurement at about half radius possibly due to a measurement error. Both models fail in reproducing the radial profile in S31, delivering a clear under-prediction in the core region and an over-prediction in the near-wall region. As the superficial gas velocity increases, the portion of BIT increases. In these cases the old BIT model (BSL-1.0) under-predicts the turbulent kinetic energy significantly while the new BIT model succeeds in reproducing the experimental data, which is seen for case S23 and case S33.

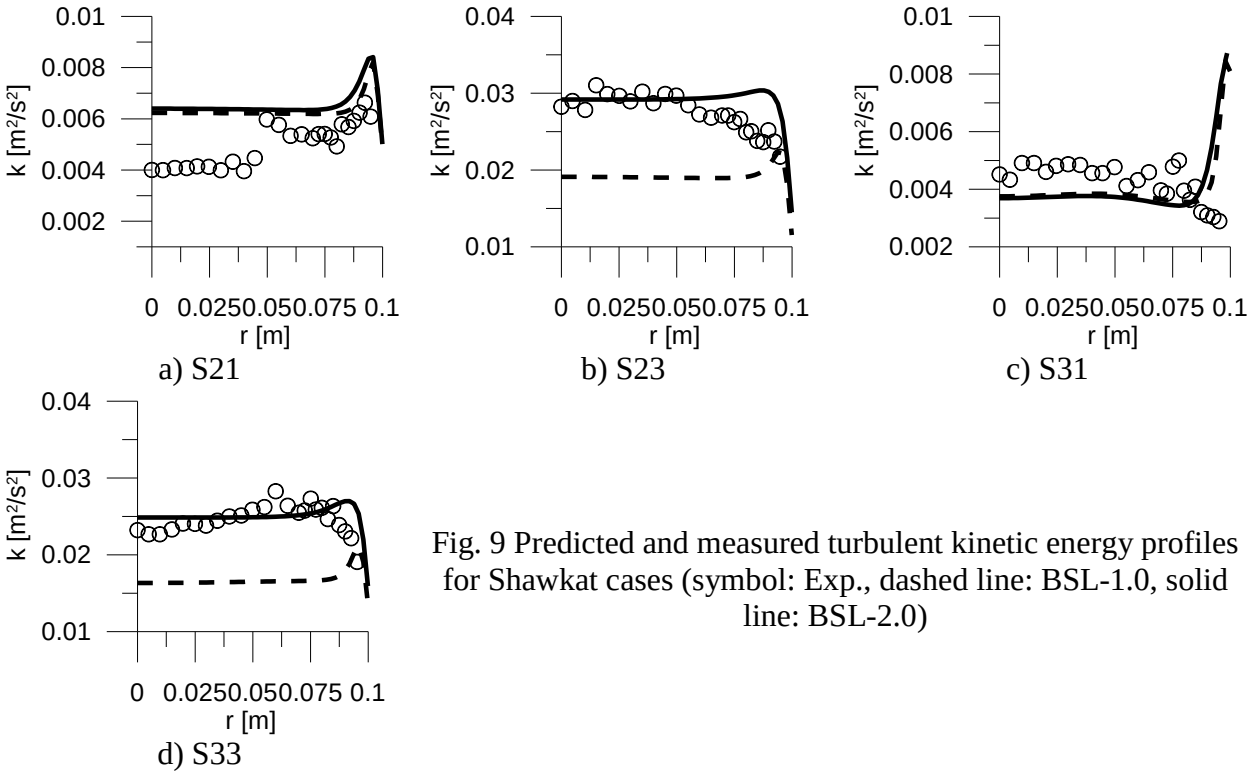

Fig. 9 Predicted and measured turbulent kinetic energy profiles for Shawkat cases (symbol: Exp., dashed line: BSL-1.0, solid line: BSL-2.0)

5.3. Ohnuki cases

A further pipe flow experiment conducted by Ohnuki and Akimoto (2000) was simulated. As shown in Table 4, the investigated case has the same superficial gas velocity as case S33 but a higher superficial liquid velocity, and consequently smaller bubble size and lower void fraction. The comparison between the predictions using the old and the new BIT model with the measurements is depicted in Fig. 10. Similar to the Shawkat cases, the void fraction distribution across the pipe is nearly uniform. A small wall-peak is observed in the experiment. Although both models over-predict the peak, the new one provides a solution obviously closer to the experimental data. Furthermore, the agreement between predicted and the measured vertical relative velocity between the gas and liquid phase is pretty good, which is important since the BIT source term in the equation for the turbulent kinetic energy is proportional to U_{rel}^3 (see Eq. 3). Despite the good prediction of the relative velocity, the BSL-1.0 model under-predict the liquid turbulent kinetic energy significantly. In contrast, the prediction provided by the new model is in quantitative agreement with the data. Furthermore, the low value given by the measurement is supposed to be caused by experimental errors, since it is significantly lower than the measurement of the similar case S33 (see Fig. 9d).

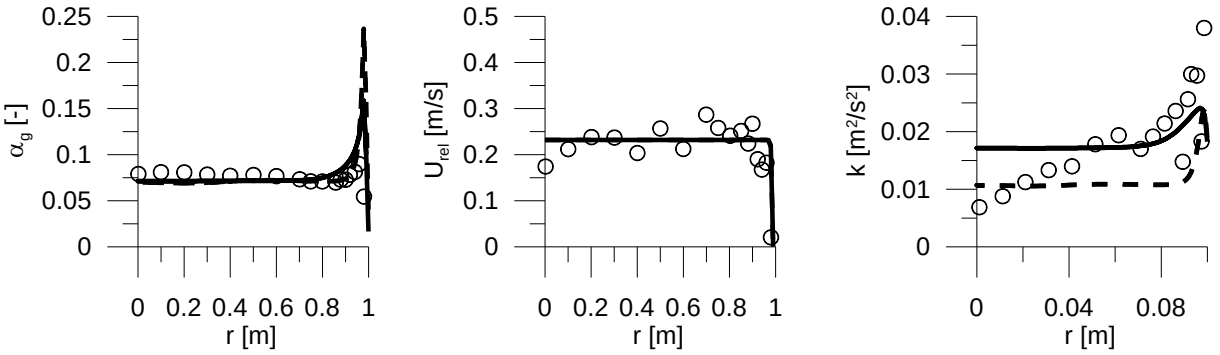

a) void fraction b) relative velocity c) turbulent kinetic energy

Fig. 10 Comparison between the simulated and measured results for the Ohnuki case (symbol: Exp., dashed line: BSL-1.0, solid line: BSL-2.0)

In summary, the comparison of the predictions for bubbly flow in pipes indicates that the performance of BSL-1.0 and BSL-2.0 is comparable in case of small bubble size and low gas volume fraction. But as the bubble size, gas volume fraction and the portion of BIT increases, the advantage of the BSL-2.0 model is obvious.

6. Results for bubble columns

Besides fully-developed pipe flow two bubble columns were simulated to check the performance of the BIT models in cases with vanishing mean liquid velocity. As shown in Table 4, the case A1 from Akbar et al. (2012) represents the homogeneous regime, while the flow in case D1 from Deen et al. (2001) is highly heterogeneous. Three-dimensional transient simulations were conducted for the two cases, and time-averaged quantities at the upper part of the column generated, i.e. at the red dashed line in Fig. 5.

6.1. Homogeneous bubble plume (case A1)

The comparison between the prediction and the measurement of radial gas volume fraction, gas and liquid velocity, and turbulent kinetic energy is shown in Fig. 11. Both models are capable of reproducing the void distribution fairly well, giving identical results for this quantity. The wall peak is over-predicted and too narrow, though. The predictions of the liquid velocity and the gas velocity also coincide between BSL-1.0 and BSL-2.0. Both are flatter than observed in the experiment. Note that the integral over the mean liquid velocity does not need to vanish in Fig. 11c) since downward flow occurs off the center plane to compensate mean upward flow along the line of data sampling. The velocity fluctuations in the simulation with the URANS consist of two parts, resolved and unresolved fluctuations. For example, the resolved part of the turbulent kinetic energy is defined as

$$k_{resolved} = \frac{1}{2}(\langle \boldsymbol{u}.\boldsymbol{u} \rangle - \langle \boldsymbol{u} \rangle.\langle \boldsymbol{u} \rangle)$$

where $\boldsymbol{u}$ is the transient velocity obtained from the URANS, and the angular brackets represent explicit time averaging. The unresolved part is provided by the turbulence model. As shown in Fig. 11d) the resolved part of the turbulent kinetic energy vanishes, while the unresolved part dominates. This is because the bubbly flow pattern in the column is uniform and stable. It is evident that the BSL-1.0 model over-predicts the turbulent kinetic energy substantially. BSL-2.0,

on the other hand, is able to capture the measured value in the column center region exactly, which is a substantial achievement. It is worth mentioning that the uniform bubble column flow is an ideal test case for BIT models in terms of turbulent kinetic energy, since the portion of shear-induced production of turbulence is negligible due to the small magnitude and the small gradients of the mean flow.

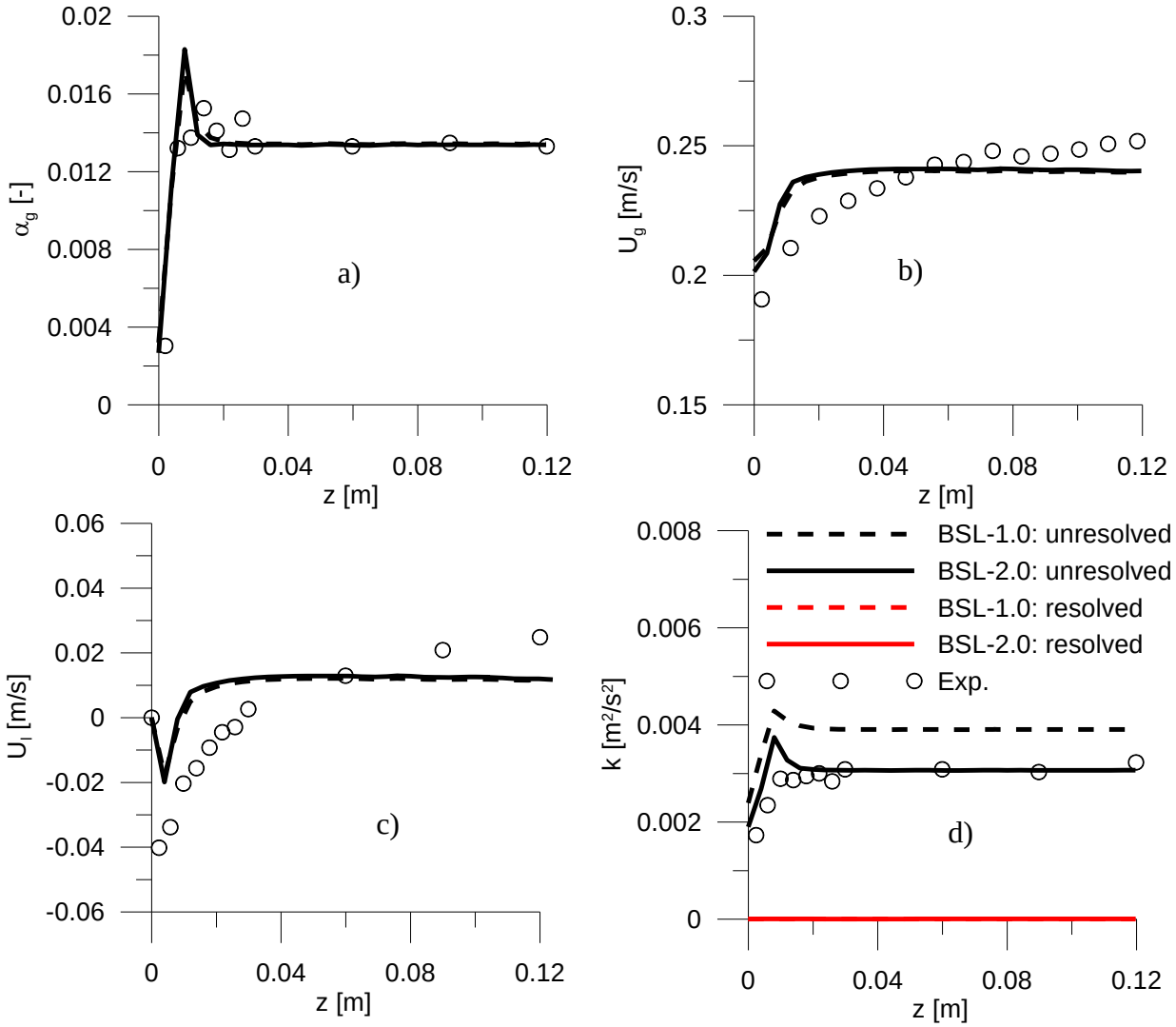

Fig. 11 Comparison between simulation results and measurement for case A1 (symbol: Exp., dashed line: BSL-1.0, solid line: BSL-2.0): a) gas volume fraction, b) axial gas velocity, c) axial liquid velocity, d) liquid turbulent kinetic energy

6.2. Oscillating bubble plume (case D1)

Figure 12 shows the results obtained with the two BIT models for the bubble column of Deen et al. (2001). In contrast to the previous case, it is characterized by an oscillating, unsteady and non-uniform bubble plume. The resolved part of the velocity fluctuations as well as the turbulent kinetic energy is both significant, even in the URANS simulations. As shown in Fig. 12a) the central gas velocity predicted by BSL-1.0 and BSL-2.0 is larger than the measured one, with that

of BSL-2.0 being much closer. The deviation in the gas velocity is related to a slight under-prediction of the drag force coefficient. The liquid velocity profile obtained with BSL-1.0 is too large while the prediction by the BSL-2.0 matches the measurement extremely well, as seen in Fig 12b). The comparison of turbulent kinetic energy and axial liquid velocity fluctuations is shown in Fig. 12c) and Fig. 12d), respectively. The red and black lines represent the resolved and unresolved parts, respectively. Obviously, the resolved axial velocity fluctuation and turbulent kinetic energy in the simulation using the BSL-2.0 are in quantitative agreement with the measurement, while a significant over-prediction in the column center is obtained with the BSL-1.0 model. Hence, the unresolved part of velocity fluctuations in this case should be fairly small. However, the predictions given by both models are non-negligible, which may be related, partly, to the over-prediction of the bubble rise velocity. In addition, turbulence dispersion affects the oscillation characteristics of the bubble plume significantly. The good agreement between the resolved velocity fluctuation profile predicted by the BSL-2.0 and the measured one evidences that the turbulence dispersion is well represented by the new model. This is consistent with the improvements observed in the radial void fraction and gas velocity profiles of the MT-Loop cases discussed above.

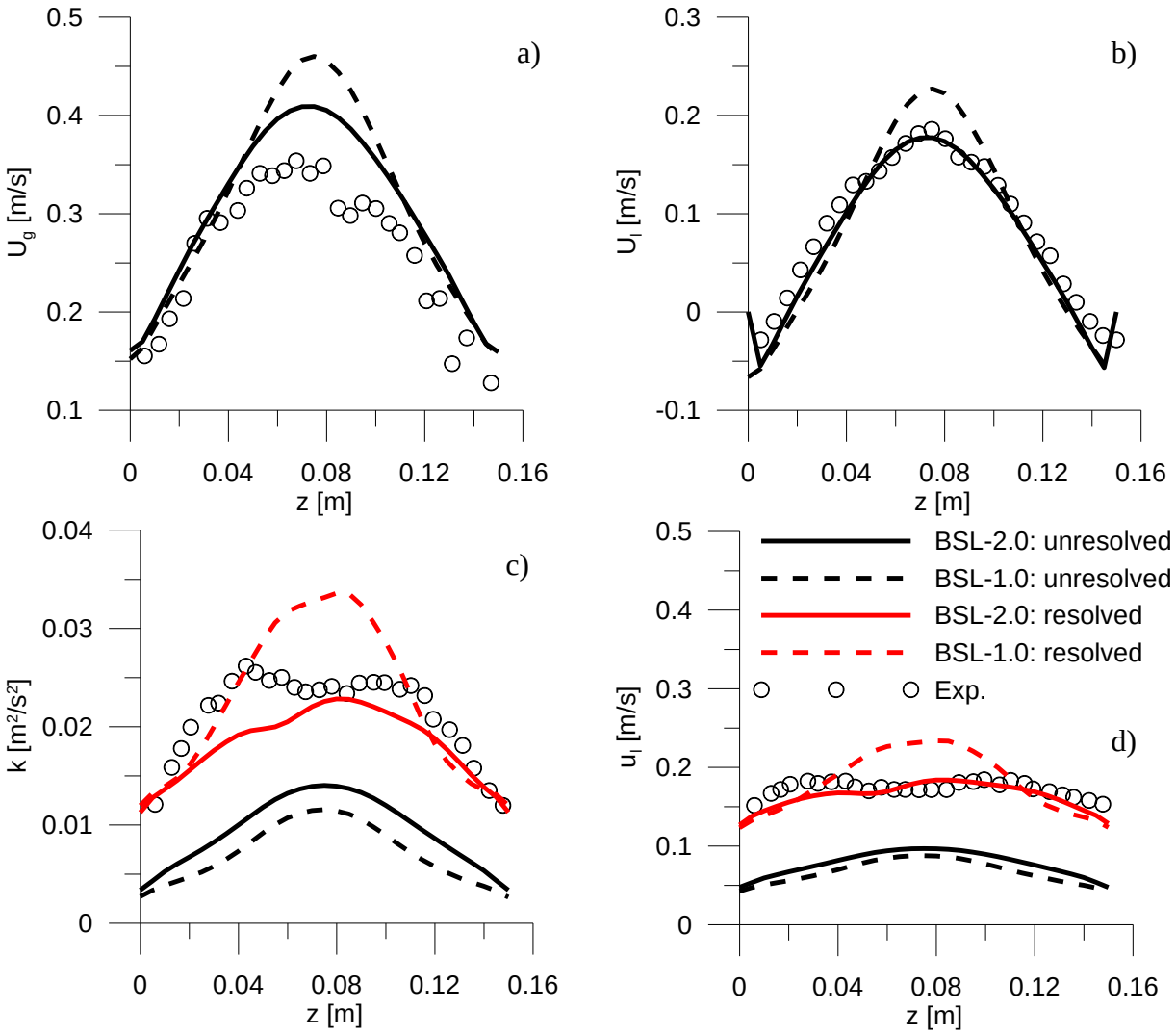

Fig. 12 Comparison between the prediction and measurement for the case D1 (symbol: Exp., dashed line: BSL-1.0, solid line: BSL-2.0): a) gas velocity, b) liquid velocity, c) liquid turbulent kinetic energy, d) axial liquid velocity fluctuation

7. Conclusions

The multi-fluid model with RANS or URANS turbulence models is a suitable tool for CFD simulations of medium and large scale bubbly flows. It provides the opportunity to account for all interfacial phenomena like BIT through closures. The generality of a closure is restricted by the degree to which the respective physical phenomenon can be specified. Unfortunately, a precise specification is often impossible due to insufficient knowledge, so that case-by-case tuning is frequently applied to get satisfying agreement with the data. Huge efforts are required to acquiring more insight into the physics of the key phenomena and to develop closures reliable over a wide range of conditions. Furthermore, a well-defined framework for the test and validation of new models is of crucial importance.

In the present work, the baseline concept of Lucas et al. (2016) was applied for the test of the BIT model recently developed by Ma et al. (2017) based on the budget analysis of the turbulent kinetic energy and its dispersion from DNS.. In the test of various cases the reference BIT sub-model was replaced by the new one, while all other sub-models as well as all constants in these sub-models remained unchanged. With this procedure, the uncertainty in tuning is reduced to a minimum. The simulation results for vertical pipe flows evidence that significant improvements regarding radial gas volume fraction and velocity profiles in high volume fraction cases are achieved with the new model. It leads to a larger eddy viscosity and, thus, to a larger turbulence dispersion, which results in a better agreement with the experimental data. Additionally, the turbulent kinetic energy in cases where BIT is dominant is predicted very well using the new BIT model, while the old one gives either an under- or an over-prediction. In summary, an overall improvement is demonstrated, so that the baseline model is now updated from the version BSL-1.0 to BSL-2.0 regarding the BIT modelling.

Nomenclature

a_1, a_3	Standard SST model constants		k	Liquid turbulent kinetic energy	$m^{-2}\cdot s^{-2}$
B_{Bi}, B_{Ci}	Birth rate of bubbles due to coalescence and breakup	$kg\cdot m^{-3}\cdot s^{-1}$	$k_{resolved}$	Resolved part of turbulent kinetic energy	$m^{-2}\cdot s^{-2}$
C_D	Drag coefficient		$k_{unresolved}$	Unresolved part of turbulent kinetic energy	$m^{-2}\cdot s^{-2}$
$C_{D,cap}$	Drag coefficient for cap bubbles		m_i, m_j	Mass of a bubble from size group i and j	kg
$C_{D,ellipse}$	Drag coefficient for ellipses		$\mathbf{n}_W$	Unit normal vector pointing away from the wall	
$C_{D,sphere}$	Drag coefficient for spheres		P_k	Turbulence shear production term	$W\cdot m^{-3}$
C_ε	Pre-factor in BIT source for ε equation		Pr_t	Turbulent Prandtl number	
$C_{\varepsilon1}$, $C_{\varepsilon2}$	Standard k-ε model constants		Re	Particle Reynolds number	
C_k	Pre-factor in BIT source for		S	An invariant measure of the	s^{-1}

	k equation			strain rate used by SST	
C_L	Lift force coefficient		S_ε	BIT source for turbulence dissipation rate	$kg \cdot m^{-1} \cdot s^{-3}$
C_μ	Standard eddy viscosity model constant		S_k	BIT source for turbulent kinetic energy	$kg \cdot m^{-1} \cdot s^{-4}$
C_{VM}	Virtual mass coefficient		S_ω	BIT source for turbulence eddy frequency	$kg \cdot m^{-3} \cdot s^{-2}$
C_W	Wall force coefficient		$\mathbf{u}_g$	Gas velocity vector	$m \cdot s^{-1}$
d	Bubble diameter, m		$\mathbf{u}_l$	Liquid velocity vector	$m \cdot s^{-1}$
d_i, d_j	Diameter of a bubble from size group i and j	m	$\mathbf{u}_{rel}$	Relative velocity vector between phases	$m \cdot s^{-1}$
D_{Bi}, D_{Ci}	Death rate of bubbles due to coalescence and breakup	$kg \cdot m^{-3} \cdot s^{-1}$	$\mathbf{u}_{rel,buoy}$	Relative velocity vector between bubbles caused by buoyancy	$m \cdot s^{-1}$
Eo	Eötvös number		$\mathbf{u}_{rel,eddy}$	Relative velocity vector between bubbles caused by shear rate inside an eddy	$m \cdot s^{-1}$
f_i	Size fraction of group i, $f_i=\alpha_i/\alpha_g$		$\mathbf{u}_{rel,shear}$	Relative velocity vector between bubbles caused by shear rate in bulk flow	$m \cdot s^{-1}$
f_1, f_2	First and second blending functions in the SST model		$\mathbf{u}_{rel,turb}$	Relative velocity vector between bubbles caused by turbulence fluctuation	$m \cdot s^{-1}$
$\mathbf{F}_D$	Interphase drag force	$kg \cdot m^{-2} \cdot s^{-2}$	$\mathbf{u}_{rel,wake,i}$	Relative velocity vector between bubble i and the bubble in its wake	$m \cdot s^{-1}$
$\mathbf{F}_L$	Shear lift force	$kg \cdot m^{-2} \cdot s^{-2}$	$\mathbf{u}_{rel,wake,j}$	Relative velocity vector between bubble j and the bubble in its wake	$m \cdot s^{-1}$
$\mathbf{F}_{TD}$	Turbulence dispersion force	$kg \cdot m^{-2} \cdot s^{-2}$	U, V, W	Components of velocity vector	$m \cdot s^{-1}$
$\mathbf{F}_{VM}$	Virtual mass force	$kg \cdot m^{-2} \cdot s^{-2}$	u, v, w	Components of velocity fluctuation vector	$m \cdot s^{-1}$
$\mathbf{F}_W$	Wall force	$kg \cdot m^{-2} \cdot s^{-2}$	X_{jki}	A matrix defining the mass division of a resultant bubble from coalescence between two adjacent size groups	
$J_{g,\,norm}$, $J_{l,norm}$	Superficial gas and liquid velocity at normal condition	$m \cdot s^{-1}$	y	The distance to nearest wall	m
$J_{g,L}$	Superficial gas velocity at Level L	$m \cdot s^{-1}$	Y_{jki}	A matrix defining the mass division of a daughter bubble from breakage between two adjacent size groups	

Greek letters

α_g, α_l	Liquid, gas volume fraction		ρ_l, ρ_g	Liquid, gas density	$kg \cdot m^{-3}$
$\alpha_{g,\,max}$	Limit of gas volume fraction		σ	Surface tension coefficient	$N\ m^{-1}$
β_3	Standard SST model constant		σ_k, σ_ε	Standard k-ε model constant	
$\Gamma(m_i, m_j)$	Coalescence rate between a bubble from size group i and a bubble from size group j	$m^3 \cdot s^{-1}$	σ_{k3}, σ_ω, $\sigma_{\omega 2}$, $\sigma_{\omega 3}$	Standard SST model constants	
Δm_{ij}	The width of size groups, special treatments necessary, see reference Liao et al. (2018)	kg	τ	Time scale for BIT destruction	s

ε	Turbulence dissipation rate	$m^2 \cdot s^{-3}$	τ_{crit}	Critical (minimum) stress for a bubble to breakup	$N \cdot m^{-2}$
η	Kolmogorov length scale	m	τ_{eddy}	Destroying stress acting on bubbles due to shear rate inside an eddy	$N \cdot m^{-2}$
Θ_i, Θ_j	Blending function in wake-entrainment coalescence, see reference Liao et al. (2015)		τ_{fric}	Destroying stress acting on bubbles due to interfacial friction	$N \cdot m^{-2}$
λ_{eff}	Effective coalescence efficiency, = $\lambda_{inertial}$ if $d_i+d_j>\eta$, otherwise = $\lambda_{viscous}$		τ_{shear}	Destroying stress acting on bubbles due to shear rate in the bulk flow	$N \cdot m^{-2}$
$\lambda_{inertial}$	Intertial bubble coalescence efficiency		τ_{turb}	Destroying stress acting on bubbles due to turbulence fluctuation	$N \cdot m^{-2}$
$\lambda_{viscous}$	Viscous bubble coalescence efficiency		ω	Turbulence eddy frequency	s^{-1}
μ_l	Molecular liquid dynamic viscosity	$Pa \cdot s$	$\Omega(m_i, m_j)$	The rate of a bubble from size group i break up into a bubble in size group j	s^{-1}
$\mu_{t,l}$	Liquid dynamic eddy viscosity	$Pa \cdot s$			
$\nu_{t,l}$	Liquid kinematic eddy viscosity	$m^2 \cdot s^{-1}$			
$\nu_{t,g}$	Gas kinematic eddy viscosity	$m^2 \cdot s^{-1}$			

References

Akbar, M. et al., 2012. Bubble tracking simulation of bubble-induced pseudoturbulence. *Multiphase Science and Technology*, 24, 197-222

Ansys, 2012. ANSYS CFX-solver theory guide, release 14.5. Canonsburg: Ansys, Inc.

Bove, S. et al., 2004. Numerical aspects of bubble column simulations. *International Journal of Chemical Reactor Engineering*, **2**, Article A1

Burns, A.D.B. et al., 2004. The Favre Averaged Drag model for turbulent dispersion in Eulerian multi-phase flows. *Proceedings of ICMF'98, 5th International Conference on Multiphase Flow,* Yokohama, Japan, May 30-June 4

Crowe, C.T. et al., 2012. *Multiphase flows with droplets and particles*, 2nd Ed., pp. 91-83, CRC Press, Boca Raton, USA.

Deen, N.G. et al., 2001. Large eddy simulation of the gas-liquid flow in a square cross-sectioned bubble column. *Chemical Engineering Science*, 56, 6341-6349

Hosokawa, S. and Tomiyama, A., 2010. Effects of bubbles on turbulent flows in vertical channels. *7th International Conference on Multiphase Flow*, Tampa, FL USA, May 30-June 4

Hosokawa, S. et al., 2002. Lateral migration of single bubbles due to the presence of wall. *Proc. ASME Joint U.S.-European Fluids Engineering Division Conference, FEDSM 2002*, Montreal, Canada

Hosokawa, S. et al., 2007. Multi-fluid simulation of turbulent bubbly pipe flows. *6th International Conference on Multiphase Flow, ICMF 2007*, Leipzig, Germany, July 9 – 13, 2007

Ilić, M., 2006. Statistical analysis of liquid phase turbulence based on direct numerical simulations of bubbly flows. *Technical report*, FZKA 7199, Forschungszentrum Karlsruhe

Ishii, M. and Zuber, N., 1979. Drag coefficient and relative velocity in bubbly, droplet or particulate flows, *AIChE J.*, **25**, 843-855
Kataoka, I. and Serizawa, A., 1989. Basic equations of turbulence in gas-liquid two-phase flow. *International Journal of Multiphase Flow*, **15**, 843-855
Kataoka, I. et al., 1993. Prediction of turbulence suppression and turbulence modeling in bubbly two-phase flow. *Nuclear Engineering and Design*, **141**, 145-158
Končar, B. et al., 2005. CFD modeling of subcooled flow boiling for nuclear engineering applications. *International Conference of Nuclear Energy for New Europe 2005*, Bled, Slovenia, September 5-8
Krepper, E., et al., 2008. The inhomogeneous MUSIG model for the simulation of polydispersed flows. *Nuclear Engineering and Design*, **238**, 1690–1702
Krepper, E. et al. 2009. CFD modelling of polydispersed bubbly two-phase flow around an obstacle. *Nuclear Engineering and Design*, **239**, 2372-2381
Krepper, E. et al., 2018. Validation of a closure model framework for turbulent bubbly two-phase flow in different flow situations. *Nuclear Engineering and Design*, **340**, 388-404
Liao, Y. et al., 2011. Development of a generalized coalescence and breakup closure for the inhomogeneous MUSIG model. *Nuclear Engineering and Design*, **241**, 1024-1033
Liao, Y. and Lucas, D., 2012 Investigations on bubble-induced turbulence modeling for vertical pipe bubbly flows. Proceedings of the 20th International Conference on Nuclear Engineering, July 30-August 3, California, USA.
Liao, Y. et al. 2015. Baseline closure model for dispersed bubbly flow: bubble coalescence and breakup. *Chemical Engineering Science*, **122**, 336-349
Liao, Y. and Lucas, D. 2016. Poly-disperse simulation of condensing steam-water flow inside a large vertical pipe. *International Journal of Thermal Sciences*, **104**, 194-207
Liao, Y., et al. 2018a. Eulerian modeling of turbulent bubbly flow based on a baseline closure concept. *Nuclear Engineering and Design,* **337**, 450-459
Liao, Y., et al. 2018b. A discrete population balance equation for binary breakage. *International Journal of Numerical Methods in Fluids*, DOI: 10.1002/fld.4491
Liu, T. J., 1998. The role of bubble size on liquid phase turbulent structure in two-phase bubbly flow. *Proceedings of the 3rd International Conference on Multiphase Flow*, ICMF1998. Lyon, France.
Lopez de Bertodano, M.A., 1992. Turbulent bubbly two-phase flow in a triangular duct. Ph.D. Dissertation, Rensselaer Polytechnic Institute.
Lucas, D. et al., 2005. Development of co-current air-water flow in a vertical pipe. *International Journal of Multiphase Flow*, **31**, 1304-1328
Lucas, D. et al., 2007. Use of models for lift, wall and turbulent dispersion forces acting on bubbles for poly-disperse flows. *Chemical Engineering Science*, **62**, 4146-4157
Lucas, D. and Tomiyama, A. 2011. On the role of the lateral lift force in poly-dispersed bubbly flows. *International Journal of Multiphase Flow*, **37**, 1178-1190
Lucas, D. et al., 2016. A strategy for the qualification of multi-fluid approaches for nuclear reactor safety. *Nuclear Engineering and Design*, **299**, 2-11
Ma, T. et al., 2017. Direct numerical simulation-based Reynolds-averaged closure for bubble-induced turbulence. *Physical Review Fluids*, **2**, 034301
Ma, T. et al., 2016. Large eddy simulations of the gas-liquid flow in a rectangular bubble column. *Nuclear Engineering and Design*, **299**, 146–153

Menter, F. R., 1994. Two-equation eddy-viscosity turbulence models for engineering applications. *AIAA-Journal,* **32**, 1598-1605
Ohnuki, A., Akimoto, H., 2001. Model development for bubble turbulent diffusion and bubble diameter in large vertical pipes. *Journal of Nuclear Science and Technology*, **38**, 1074–7080
Pan, Y. et al., 1999. Dynamic simulation of bubbly flow in bubble columns, Chemical Engineering Science, **54**, 2481-2489
Pfleger, D. and Becker, S., 2001. Modelling and simulation of the dynamic flow behaviour in a bubble column. *Chemical Engineering and Science*, **56**, 1737-1747
Politano, M.S. et al., 2003. A model for turbulent polydisperse two-phase flow in vertical channels. *International Journal of Multiphase flow*, **29**, 1153-1182
Prasser, H.-M. et al., 2003. Flow maps and models for transient two-phase flows. Technical report, 150 1215, Helmholtz-Zentrum Dresden-Rossendorf
Rabha, S. et al., 2013. Intrinsic flow behavior in a slurry bubble column: A study on the effect of particle size. *Chemical Engineering Science*, **93**, 401-411
Rzehak, R. and Krepper, E. 2013. CFD modeling of bubble-induced turbulence. *International Journal of Multiphase Flow*, **55**, 138-155
Rzehak, R., et al., 2017. Unified modeling of bubbly flows in pipes, bubble columns, and airlift columns. *Chemical Engineering Science*, **157**, 147-158
Santarelli, C. and Fröhlich, J., 2016. Direct numerical simulations of spherical bubbles in vertical turbulent channel flow: Influence of bubble size and bidispersity. *International Journal of Multiphase Flow*, **81**, 27-45
Santarelli, C. et al., 2016. Budget analysis of the turbulent kinetic energy for bubbly flow in a vertical channel, Chemical Engineering Science, **141**, 46-62
Sato, Y. and Sekoguchi, K., 1975. Liquid velocity distribution in two-phase bubble flow, International Journal of Multiphase Flow, **2**, 79–95
Scott, D. et al., 2004. CFD model of an aerating hydrofoil. *IOP Conference Series: Earth and Environmental Science*, **22**, 062008
Shawkat, M., et al., 2008. Bubble and liquid turbulence character- istics of bubbly flow in a large diameter vertical pipe. *International Journal Multiphase Flow*, **34**, 767–785
Troshko, A. A. and Hassan, Y. A., 2001. A two-equation model of turbulent bubbly flows. *International Journal of Multiphase Flow*, **27**, 1965-2000
Tomiyama, A., et al. 2002. Transverse migration of single bubbles in simple shear flows. Chemical Engineering Science, 57, 1849 – 1858
Vaidheeswaran, A. and Hibiki, T., 2017. Bubble-induced turbulence modeling for vertical bubbly flows. *International Journal of Heat and Mass Transfer*, **115**, 741-752
Yao, W. and Morel, C., 2004. Volumetric interfacial area prediction in upward bubbly two-phase flow. International Journal of Heat and Mass Transfer, **47**, 307-328
Ziegenhein, T., et al. 2017. Towards a unified approach for modelling uniform and non-uniform bubbly flows. *The Canadian Journal of Chemical engineering*, **95**, 170-179